PHYSICAL REVIEW C **74**, 021901(R) (2006)

Charged-particle pseudorapidity distributions in Au+Au collisions at $\sqrt{s_{NN}} = 62.4$ GeV

B. B. Back,[1] M. D. Baker,[2] M. Ballintijn,[4] D. S. Barton,[2] R. R. Betts,[6] A. A. Bickley,[7] R. Bindel,[7] W. Busza,[4] A. Carroll,[2] Z. Chai,[2] M. P. Decowski,[4] E. García,[6] T. Gburek,[3] N. George,[2] K. Gulbrandsen,[4] C. Halliwell,[6] J. Hamblen,[8] M. Hauer,[2] C. Henderson,[4] D. J. Hofman,[6] R. S. Hollis,[6] R. Hołyński,[3] B. Holzman,[2] A. Iordanova,[6] E. Johnson,[8] J. L. Kane,[4] N. Khan,[8] P. Kulinich,[4] C. M. Kuo,[5] W. T. Lin,[5] S. Manly,[8] A. C. Mignerey,[7] R. Nouicer,[2,6] A. Olszewski,[3] R. Pak,[2] C. Reed,[4] C. Roland,[4] G. Roland,[4] J. Sagerer,[6] H. Seals,[2] I. Sedykh,[2] C. E. Smith,[6] M. A. Stankiewicz,[2] P. Steinberg,[2] G. S. F. Stephans,[4] A. Sukhanov,[2] M. B. Tonjes,[7] A. Trzupek,[3] C. Vale,[4] G. J. van Nieuwenhuizen,[4] S. S. Vaurynovich,[4] R. Verdier,[4] G. I. Veres,[4] E. Wenger,[4] F. L. H. Wolfs,[8] B. Wosiek,[3] K. Woźniak,[3] and B. Wysłouch[4]

(PHOBOS Collaboration)

[1]*Argonne National Laboratory, Argonne, Illinois 60439-4843, USA*

[2]*Brookhaven National Laboratory, Upton, New York 11973-5000, USA*

[3]*Institute of Nuclear Physics, PAN, Kraków, Poland*

[4]*Massachusetts Institute of Technology, Cambridge, Massachusetts 02139-4307, USA*

[5]*National Central University, Chung-Li, Taiwan*

[6]*University of Illinois at Chicago, Chicago, Illinois 60607-7059, USA*

[7]*University of Maryland, College Park, Maryland 20742, USA*

[8]*University of Rochester, Rochester, New York 14627, USA*

(Received 26 September 2005; published 10 August 2006)

The charged-particle pseudorapidity density for Au+Au collisions at $\sqrt{s_{NN}} = 62.4$ GeV has been measured over a wide range of impact parameters and compared to results obtained at other energies. As a function of collision energy, the pseudorapidity distribution grows systematically both in height and width. The midrapidity density is found to grow approximately logarithmically between BNL Alternating Gradient Synchrotron (AGS) energies and the top BNL Relativistic Heavy Ion Collider (RHIC) energy. There is also an approximate factorization of the centrality and energy dependence of the midrapidity yields. The new results at $\sqrt{s_{NN}} =$ 62.4 GeV confirm the previously observed phenomenon of "extended longitudinal scaling" in the pseudorapidity distributions when viewed in the rest frame of one of the colliding nuclei. It is also found that the evolution of the shape of the distribution with centrality is energy independent, when viewed in this reference frame. As a function of centrality, the total charged particle multiplicity scales linearly with the number of participant pairs as it was observed at other energies.

DOI: 10.1103/PhysRevC.74.021901 PACS number(s): 25.75.Dw

In previous publications the PHOBOS Collaboration has presented the full systematic behavior of inclusive charged particle production in heavy ion collisions over a large range of collision parameters: (1) $\sqrt{s_{NN}}$ from 19.6 GeV to 200 GeV, (2) pseudorapidities from $\eta = -5.4$ to 5.4, nearly the full solid angle, and 3) average impact parameter from $\langle b \rangle =$ 3–10.5 fm, corresponding to 50–360 participating nucleons (N_{part}) [1–7]. While these data are already useful as a broad systematic study, several nontrivial features have been made manifest by direct comparisons between the data at different energies and centralities: (1) a logarithmic increase with $\sqrt{s_{NN}}$ in the midrapidity particle density [2], (2) an approximate factorization of the centrality and energy dependence of the midrapidity yields [7], (3) the phenomenon of "limiting fragmentation" in the forward direction [6], and (4) a linear "N_{part}-scaling" of the total particle yield [8]. This paper presents for the first time the multiplicity data for Au+Au collisions at the most recent BNL Relativistic Heavy Ion Collider (RHIC) energy of $\sqrt{s_{NN}} = 62.4$ GeV, corresponding to the top energy reported by several earlier $p + p$ experiments at the CERN Intersecting Storage Rings (ISR). With our new data, we can test the previously-found scaling relationships at an intermediate energy.

The data were obtained with the PHOBOS detector [9] during the RHIC 2004 run. In this analysis only the data taken with the magnetic field switched off are analyzed. To select events with various ranges of impact parameter, characterized typically by N_{part}, we use the particle multiplicity measured in two sets of "paddle" counters, situated at $z = \pm 3.21$ meters from the nominal interaction point. These cover a pseudorapidity range of $3.2 < |\eta| < 4.5$ with 95% azimuthal acceptance. The overall triggering and event selection efficiency at 62.4 GeV corresponds to $81 \pm 2\%$ of the total Au+Au inelastic cross section, estimated using HIJING simulations [10]. We use the Glauber model calculation implemented in HIJING to estimate $\langle N_{\text{part}} \rangle$ for each centrality bin by assuming a monotonic relationship between N_{part} and the relevant experimental observable. This procedure has been described in Refs. [1,4,5]. It was found that trigger efficiencies are typically around 100% for the top 50% of the total cross section at energies of $\sqrt{s_{NN}} = 62.4$, 130, and 200 GeV. At the lowest energy of $\sqrt{s_{NN}} = 19.6$ GeV, an alternative method of centrality determination was developed, that uses all particles detected in the "Octagon" silicon detector, covering $|\eta| < 3$, as a measure of the particle multiplicity [6]. These two methods agree within 3% at the higher energies and have been used

TABLE I. Data for Au+Au collisions at $\sqrt{s_{NN}} = 62.4$ GeV including $dN_{\rm ch}/d\eta|_{|\eta|<1}$, $dN_{\rm ch}/d\eta|_{|\eta|<1}/\langle N_{\rm part}/2\rangle$ as shown in Fig. 4 and $\langle N_{\rm ch}\rangle$ and $\langle N_{\rm ch}\rangle/\langle N_{\rm part}/2\rangle$ as shown in Fig. 7. The difference in $N_{\rm part}$ in the 0%–3% bin is explained in the text.

Centrality		Fig. 4		Fig. 7	
Bin	$N_{\rm part}$	$dN_{\rm ch}/d\eta$ ($\lvert\eta\rvert < 1$)	$dN_{\rm ch}/d\eta/\langle N_{\rm part}/2\rangle$	$N_{\rm ch}$	$N_{\rm ch}/\langle N_{\rm part}/2\rangle$
0–3%	356 ± 11	492 ± 36	2.76 ± 0.23		
	349 ± 11			2988 ± 149	17.10 ± 1.11
3–6%	325 ± 10	433 ± 32	2.67 ± 0.22	2775 ± 138	17.17 ± 0.91
6–10%	288 ± 9	377 ± 28	2.62 ± 0.21	2489 ± 124	17.29 ± 0.94
10–15%	248 ± 8	316 ± 23	2.55 ± 0.21	2120 ± 106	17.13 ± 1.00
15–20%	209 ± 7	260 ± 19	2.50 ± 0.20	1777 ± 88	17.03 ± 1.11
20–25%	174 ± 7	212 ± 15	2.44 ± 0.21	1485 ± 74	17.07 ± 1.27
25–30%	145 ± 7	174 ± 13	2.41 ± 0.21	1236 ± 61	17.03 ± 1.46
30–35%	119 ± 7	140 ± 10	2.35 ± 0.22	1027 ± 51	17.15 ± 1.67
35–40%	98 ± 7	111 ± 8	2.28 ± 0.23	840 ± 42	17.17 ± 1.90
40–45%	78 ± 6	87 ± 6	2.24 ± 0.25	679 ± 33	17.30 ± 2.12
45–50%	62 ± 6	67 ± 5	2.16 ± 0.26	532 ± 26	17.16 ± 2.29

as a cross-check in this analysis. However it should be noted that the two methods give values of $\langle N_{\rm part}\rangle$ that differ by 2% in the most central bin, since this bin is more sensitive to the fluctuations of the variable used to estimate the centrality. Thus, we separate the tabulated results (in Table I) for that bin, but do not in the other bins when they agree to better than 1%.

Several methods were used to estimate the charged particle density in each centrality class. In the full phase space, a combination of data from the single-layer "Octagon" ($|\eta| < 3$) and "Ring" ($3 < |\eta| < 5.4$) detectors were analyzed using two different techniques. In the "analog" method, the deposited energy in a detector pad is used to estimate the number of particles traversing the pad after accounting for orientation of the Si-wafer relative to the interaction point. The "digital" approach treats each pad as a binary counter and assumes Poisson statistics to estimate the total occupancy in various regions of pseudorapidity. These methods have been discussed in more detail in Refs. [3] and [6]. At midrapidity, the PHOBOS vertex detector, consisting of two planes covering $|\eta| < 0.92$ over a limited azimuthal range, $\Delta\phi \sim 90^\circ$, is used to count "tracklets". These are two-hit tracks which point back to the event vertex, providing redundancy not present in the single-layer analyses, and thereby reducing systematic effects at midrapidity. This method has been described in detail in Refs. [3,5,7]. It should be emphasized that the silicon detectors are sensitive to most of the particles produced in the collision, down to $p_T = 4$ MeV/c (10 MeV/c) at $\eta \sim 4$–5, and 35 MeV/c (140 MeV/c) at midrapidity for pions (protons).

The $\sqrt{s_{NN}} = 62.4$ GeV data are shown in Fig. 1 as a function of collision centrality, determined by the paddle-counter method. Results using the Octagon-based centrality method, shown for each bin by dotted lines, agree very well with those from the paddle-based method. Midrapidity data from the tracklet method also agree well with the single-Si-layer analysis over the full centrality range studied.

To place these data in context, Fig. 2 shows data from the 6% most central collisions in comparison with similar data at 19.6, 130, and 200 GeV from Ref. [6]. Increases both in the height and width of the distribution are observed as a function of increasing energy. Already at $\sqrt{s_{NN}} = 62.4$ GeV, the central

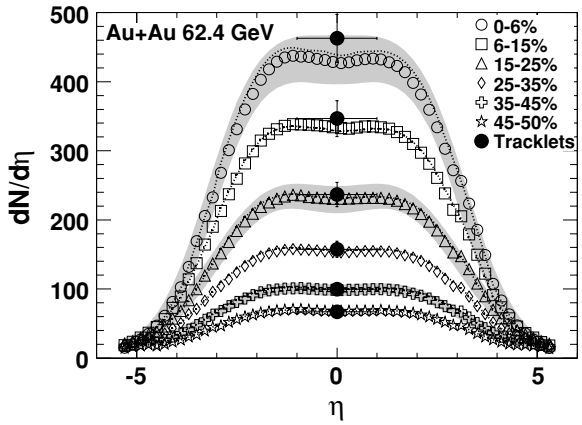

FIG. 1. Pseudorapidity distributions $dN_{\rm ch}/d\eta$ from Au+Au collisions at $\sqrt{s_{NN}} = 62.4$ GeV. Open symbols show the results obtained using the paddle-based centrality method with 90% C. L. systematic errors indicated by grey bands for selected bins. The dotted lines show the results obtained using the "Octagon"-based centrality method. The filled circles show the average value of $dN_{\rm ch}/d\eta|_{|\eta|<1}$ using the tracklet technique, with the horizontal bars indicating the interval in η over which the averaging is done. The centrality is denoted by the fraction of the total inelastic cross section, with smaller numbers corresponding to more central events.

"plateau" nascent at $\sqrt{s_{NN}} = 19.6$ GeV is fully developed and grows in width slowly with increasing energy. Of course, the existence of a plateau in $dN_{\rm ch}/d\eta$ does not necessarily imply the existence of a plateau in dN/dy because of the nontrivial transformation between rapidity and pseudorapidity ($dy = \beta d\eta$) [6].

The scaled particle densities near midrapidity ($dN_{\rm ch}/d\eta|_{|\eta|<1}/\langle N_{\rm part}/2\rangle$) for $\sqrt{s_{NN}} = 19.6$, 130, and 200 GeV [1,2,4–7,12] are shown as a function of collision energy in Fig. 3 for the 6% most central events. Where possible, PHOBOS results from the various measurement techniques have been averaged at each energy, weighted by the inverse square of the relative error. At $\sqrt{s_{NN}} = 62.4$ GeV, this gives $dN_{\rm ch}/d\eta|_{|\eta|<1}/\langle N_{\rm part}/2\rangle = 2.64 \pm 0.18$. Data from compara-

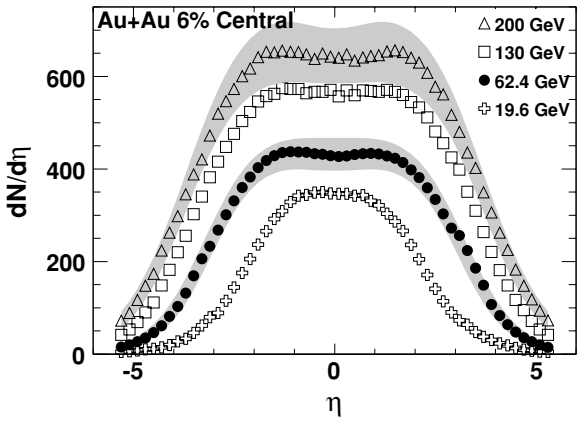

FIG. 2. The pseudorapidity distributions measured in the 6% most-central Au+Au collisions at four RHIC energies. 90% C. L. systematic errors are shown as grey bands.

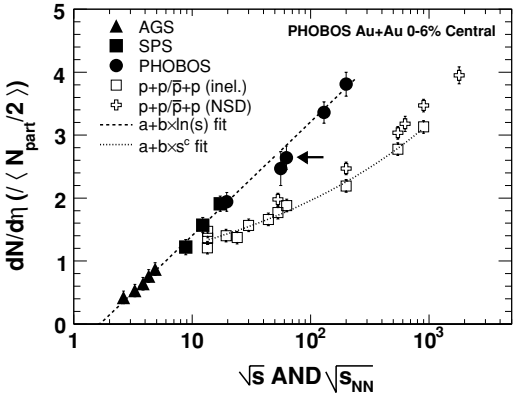

FIG. 3. $dN_{\rm ch}/d\eta|_{|\eta|<1}/\langle N_{\rm part}/2\rangle$ shown for Au+Au collisions as a function of energy. The PHOBOS data, averaged over all available measurement techniques, is compared with lower-energy $A+A$ data as well as a variety of $p+p$ and $\overline{p}+p$ data. The thick dashed line is a fit ($a+b\ln(s)$, with $a=-0.40$ and $b=0.39$) to the $\sqrt{s_{NN}}=$ 19.6, 130, and 200 GeV data points. The inelastic $p+p$ and $\overline{p}+p$ data have been fit by a function $a+bs^c$ (with $a=0.35$, $b=0.52$ and $c=0.12$), shown by a thin dotted line.

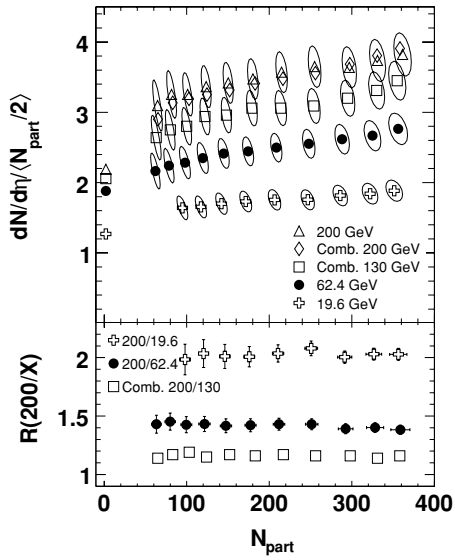

FIG. 4. (a) $dN_{\rm ch}/d\eta|_{|\eta|<1}/\langle N_{\rm part}/2\rangle$ measured using the tracklet technique as a function of $N_{\rm part}$ for four RHIC energies ($\sqrt{s_{NN}}=$ 19.6, 62.4, 130, and 200 GeV). Also shown are inelastic $p+p$ data for $\sqrt{s}=62.4$ and $\sqrt{s}=200$ GeV, and interpolated values for $\sqrt{s}=19.6$ GeV (Ref. [7]) and $\sqrt{s}=130$ GeV (using the fit shown in Fig. 3). The systematic errors are shown as 90% C. L. ellipses (reflecting the trivial correlation in $dN_{\rm ch}/d\eta|_{|\eta|<1}/\langle N_{\rm part}/2\rangle$ and $N_{\rm part}$). (b) The ratio of the scaled pseudorapidity densities measured at 200 GeV to those measured at $\sqrt{s_{NN}}=19.6$, 62.4, and 130 GeV.

ble centralities at lower energies are also shown, as compiled in Ref. [12]. While high-statistics data from the three other RHIC energies suggested an approximately-logarithmic rise of the particle density, the low-statistics data point measured at $\sqrt{s_{NN}}=56$ GeV was found to be only barely consistent with a logarithmic fit based only on the data at $\sqrt{s_{NN}}=19.6$, 130, and 200 GeV (shown as a dashed line). The data point at $\sqrt{s_{NN}}=62.4$ GeV (indicated by an arrow in Fig. 3) falls closer to the fit, and is, within errors, consistent with the logarithmic rise. The $A+A$ data are compared to a wide range of $p+p$ and $\overline{p}+p$ data, separately shown for inelastic as well as nonsingle diffractive events [13–15]. While these data also appear to rise logarithmically at higher energies, the inclusion of data points below $\sqrt{s}\sim 30$ GeV appears to indicate a curvature in the energy dependence. To interpolate between the measured points, they have been fit by a function $a+bs^c$, shown by the thin dotted line.

The centrality dependence of $dN_{\rm ch}/d\eta|_{|\eta|<1}/\langle N_{\rm part}/2\rangle$, measured with the tracklet technique, is shown in Fig. 4(a), and tabulated in Table I. Data at $\sqrt{s_{NN}}=19.6$, 62.4, and 200 GeV have been analyzed using only the tracklet technique in the PHOBOS Vertex detector (hereafter called the "vertex-tracklet" method) and the Octagon-based centrality method. At 130 and 200 GeV, results are also available using a method (the "combined" method) which averages the vertex tracklet results with a similar method using the PHOBOS spectrometer [5], and using the paddle-based centrality method. The results are typically compatible within 2% over the full centrality range, as can be seen by direct comparison in Fig. 4(a) of the vertex tracklet and the combined result for 200 GeV. The vertex-tracklet method and Octagon-based centrality method is used at 62.4 GeV for overall consistency and partial cancellation of certain systematics in the ratios relative to 19.6 and 200 GeV data.

The centrality dependence of the mid-rapidity yields has often been interpreted in a two-component picture of particle production, with "soft" processes scaling with $N_{\rm part}$ and "hard" processes scaling with the number of binary collisions, $N_{\rm coll}$. In $p+p$ collisions, particle production from hard and semi-hard processes is expected to eventually dominate over that from soft processes as the minijet cross sections increase [10] with increasing beam energy. In Au+Au collisions, the number of binary collisions exceeds the number of participant pairs by a factor ranging from near 1 in very peripheral events, to ~5–6 in central events. Combining these effects, one might expect a progressively steeper centrality dependence of the scaled yields as the beam energy increases. This expectation may be tested by studying the ratio of the yields at different energies for the same fraction of the total cross section, shown in Fig. 4(b). Despite the expected increase in hard processes with increasing energy, these ratios are observed to be constant over the measured centrality range, showing a "factorization" of beam energy and collision geometry at midrapidity. This result extends the analysis presented in Ref. [7] and is fully compatible with the constant ratio found in comparisons between data at $\sqrt{s_{NN}}=200$ and 130 GeV obtained with the "combined" method. All of these data suggest that while two-component models can fit the midrapidity data at each energy, they do not have an energy dependence characteristic of a growing contribution of hard-processes. PHENIX data taken at different energies [11] qualitatively agrees with these conclusions.

In a previous PHOBOS publication, the phenomenon of "limiting fragmentation" was observed by comparing Au+Au collisions at the three RHIC energies for which 4π data were

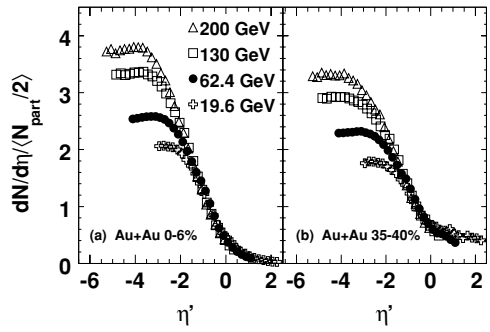

FIG. 5. The scaled pseudorapidity density ($dN_{\rm ch}/d\eta/\langle N_{\rm part}/2\rangle$) for two centrality bins (0–6% and 35–40%) and four RHIC energies shown in the rest frame of one of the projectiles by using the variable $\eta' = \eta - y_{\rm beam}$. For clarity, systematic errors are not shown in this figure.

available [6]. This phenomenon, which we also refer to as "extended longitudinal scaling" [16] is simply the invariance of the scaled yields $dN_{\rm ch}/d\eta/\langle N_{\rm part}/2\rangle$ with beam energy in the reference frame of one of the projectiles, i.e., by plotting the scaled yields with respect to the variable $\eta' = \eta - y_{\rm beam}$, where $y_{\rm beam}$ is the beam rapidity. The concept of extended longitudinal scaling is expected to apply to rapidity distributions, but since $\eta \sim y - \ln(p_T/m_T)$ for particles emitted far away from midrapidity, this scaling is also expected to apply to pseudorapidity distributions. This scaling phenomenon was also found in d+Au collisions at RHIC [16] and, surprisingly, also for elliptic flow at all of the RHIC energies, including $\sqrt{s_{NN}} = 62.4$ GeV [17]. The new multiplicity data at $\sqrt{s_{NN}} =$ 62.4 GeV, shown in Figs. 5(a) and 5(b), clearly fit well into the existing pattern.

The data in Fig. 5 suggest that the shape of $dN_{\rm ch}/d\eta$ (away from midrapidity) is mainly a function of the collision geometry rather than of the beam energy, when observed in the rest frame of one of the projectiles. While one cannot rule out a small energy dependence in the forward region, the size of the systematic errors preclude any definitive statements based on these data. The energy-independence of the change in shape is shown more clearly in Fig. 6, where the ratio of peripheral to central data scaled by $N_{\rm part}$

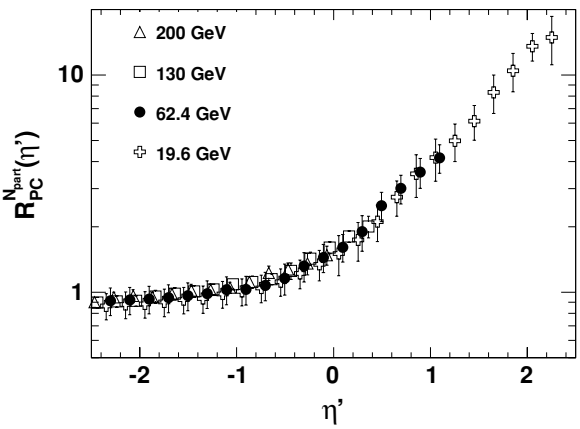

FIG. 6. $R_{PC}^{N_{\rm part}}$ as a function of η' comparing the 35–40% bin to the 0–6% most central bin for four different energies.

$$R_{PC}^{N_{\rm part}}(\eta', 35\text{–}40\%) = \frac{N_{\rm part}^{0-6\%}}{N_{\rm part}^{35-40\%}} \frac{dN_{\rm ch}/d\eta^{35-40\%}}{dN_{\rm ch}/d\eta^{0-6\%}}$$

is plotted as a function of η'. The error bars in this figure indicate 90% C. L. systematic errors. A similar figure was shown in Ref. [6], showing that the change in shape as a function of centrality is independent of beam energy when observed in the rest frame of one of the projectiles. The STAR experiment has measured photons in $-1.9 < \eta' < -0.5$ and reported no significant dependence [20] on the energy and centrality. We observe that even the inclusive charged particles have little variation in this region, as shown in Fig. 6, suggesting that these data sets are quite compatible. The ratio $R_{N_{\rm part}}^{PC}$ was also used to compare the shapes of transverse momentum distributions, dN/dp_T, measured near midrapidity for different energies and centralities, and a similar invariance with energy was found for each centrality bin [18], i.e., in all of these cases, the centrality and energy dependences factorize to a large extent. Such behavior has also been seen in proton-nucleus collisions at lower energies [19].

As observed previously, the centrality dependence of the limiting curve has the interesting property that the decrease in the scaled particle density, $dN_{\rm ch}/d\eta/\langle N_{\rm part}/2\rangle$, at midrapidity when moving from central to peripheral events is correlated with the increase at forward rapidities. Although some of the particles with $\eta' > 0$ may be attributed to emission from spectators, the systematic change of the slope leads to an approximately constant total multiplicity. Using the method outlined in Ref. [8], which combines analytic fits of the measured region with estimates of the unmeasured yields using the lower-energy data, the total charged-particle multiplicity extrapolated to 4π has been calculated as a function of centrality, as shown in Fig. 7 and tabulated in Table I. The uncertainty from the extrapolation procedure itself is indicated by the grey bands. As at the other RHIC energies [8], the data at $\sqrt{s_{NN}} = 62.4$ GeV shows an approximately linear relationship between $N_{\rm ch}$ and $N_{\rm part}$. This persistence of "wounded nucleon scaling" [21,22] has not been fully explained for heavy ion collisions, especially since the multiplicity is evidently not a simple multiplication of nucleon-nucleon multiplicity by $N_{\rm part}/2$.

It is an interesting question whether or not the various scaling behaviors discussed, such as the factorization of energy and geometry at midrapidity (Fig. 4) and the similar factorization of the distributions in η' (Fig. 6), should be considered independent phenomena. Already, the $N_{\rm part}$ scaling shown in Fig. 7 suggests that modifications to particle production at forward rapidities are strongly correlated with compensating changes at midrapidity. If, in fact, the pseudorapidity distribution at each energy deviates from the limiting curve by flattening out at the same value of η at all centralities, then the factorization of energy and geometry at midrapidity follows naturally as a consequence of the centrality dependence of the energy-independent limiting curve. Figure 5 suggests that this

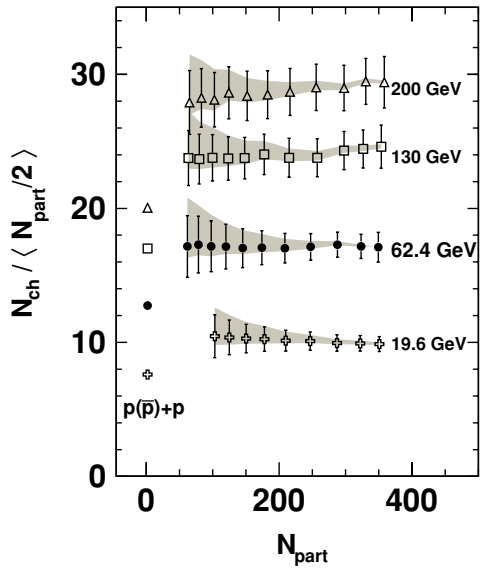

FIG. 7. $\langle N_{\rm ch}\rangle/\langle N_{\rm part}/2\rangle$, obtained by extrapolating the data at each energy into the unmeasured region, as a function of centrality. The 90% C. L. uncertainty on $N_{\rm ch}$ and $N_{\rm part}$ have been combined into the error bars, while the 90% C. L. uncertainty on the extrapolation procedure is indicated by a grey band. Inelastic $p+p$ and $\overline{p}+p$ data, all interpolated using a power-law fit ($N_{\rm ch} = -4.2 + 4.69s^{0.155}$, from Ref. [14]) are shown at $N_{\rm part} = 2$.

deviation is centrality independent, within the experimental uncertainties, and the flat ratios displayed in Fig. 4 at least show that its centrality dependence is energy-independent. Now, if the deviation also occurs in an energy-independent location in η, this would connect the approximately logarithmic energy dependence (Fig. 3) to the shape of the limiting curve in central events. Indeed, Fig. 2 suggests that the spectra flatten out at $\eta \sim 1.5$–2 (except perhaps at the lowest RHIC energy). Of course, empirical observations like these do not *explain* why these relationships between the various regions of phase space hold, but rather point to issues that need to be addressed in the global understanding of heavy ion collisions. It would be interesting to see similar studies (of energy *and* centrality dependence) performed on STAR and PHENIX data on identified particle yields, which appear to vary with centrality in different ways, as, e.g., shown by STAR for $K^\star$ production [23]. It is possible that they behave similarly to the results shown here on inclusive charged-particle yields, which could give insight into the general mechanism of particle production in these systems.

In summary, the charged-particle pseudorapidity density has been measured by PHOBOS for Au+Au collisions at $\sqrt{s_{NN}} = 62.4$ GeV, matching the top ISR energy. As a function of collision energy, the pseudorapidity distribution grows systematically both in height and width. The midrapidity density is found to grow approximately logarithmically between AGS energies and the top RHIC energy. There is an approximate factorization of the centrality dependence of the mid-rapidity yields and the energy-dependent overall multiplicity scale. The phenomenon of "extended longitudinal scaling" (also known as "limiting fragmentation") is clearly present in the 62.4 GeV data. Finally, a relatively-small extrapolation of the measured yields to 4π allows the extraction of the total charged-particle multiplicity. As at the other RHIC energies, $N_{\rm ch}$ is found to scale approximately linearly with the number of participants over the range of collision centralities studied.

This work was partially supported by U.S. DOE grants DE-AC02-98CH10886, DE-FG02-93ER40802, DE-FC02-94ER40818, DE-FG02-94ER40865, DE-FG02-99ER41099, and W-31-109-ENG-38, by U.S. NSF grants 9603486, 0072204, and 0245011, by Polish KBN grant 1-P03B-062-27(2004-2007), by NSC of Taiwan Contract NSC 89-2112-M-008-024, and by Hungarian OTKA grant (F 049823).

[1] B. B. Back *et al.*, Phys. Rev. Lett. **85**, 3100 (2000).
[2] B. B. Back *et al.*, Phys. Rev. Lett. **88**, 022302 (2002).
[3] B. B. Back *et al.*, Phys. Rev. Lett. **87**, 102303 (2001).
[4] B. B. Back *et al.*, Phys. Rev. C **65**, 031901(R) (2002).
[5] B. B. Back *et al.*, Phys. Rev. C **65**, 061901(R) (2002).
[6] B. B. Back *et al.*, Phys. Rev. Lett. **91**, 052303 (2003).
[7] B. B. Back *et al.*, Phys. Rev. C **70**, 021902(R) (2004).
[8] B. B. Back *et al.*, arXiv:nucl-ex/0301017.
[9] B. B. Back *et al.*, Nucl. Instrum. Methods A **499**, 603 (2003).
[10] M. Gyulassy and X. N. Wang, Comput. Phys. Commun. **83**, 307 (1994).
[11] S. S. Adler *et al.*, Phys. Rev. C **71**, 034908 (2005) [Erratum-*ibid.***71**, 049901 (2005)].
[12] B. B. Back *et al.*, Nucl. Phys. **A757**, 28 (2005).
[13] G. J. Alner *et al.*, Z. Phys. C **33**, 1 (1986).
[14] H. Heiselberg, Phys. Rep. **351**, 161 (2001).
[15] F. Abe *et al.*, Phys. Rev. D **41**, 2330 (1990).
[16] B. B. Back *et al.*, Phys. Rev. C **72**, 031901(R) (2005).
[17] B. B. Back *et al.*, Phys. Rev. Lett. **94**, 122303 (2005).
[18] B. B. Back *et al.*, Phys. Rev. Lett. **94**, 082304 (2005).
[19] W. Busza, Nucl. Phys. **A544**, 49 (1992).
[20] J. Adams *et al.*, Phys. Rev. Lett. **95**, 062301 (2005).
[21] J. E. Elias *et al.*, Phys. Rev. Lett. **41**, 285 (1978).
[22] A. Białas, B. Bleszyński, and W. Czyż, Nucl. Phys. **B111**, 461 (1976).
[23] J. Adams *et al.*, Phys. Rev. C **71**, 064902 (2005).